Giant response to spin-orbit torques in heavy-metal/ferromagnetic bilayers associated with magnetic reversal

Ariel Zaig●, Shubhankar Das●, Moty Shultz, and Lior Klein●

Department of Physics, Nano-magnetism Research Center, Institute of Nanotechnology and Advanced Materials,
Bar-Ilan University, Ramat-Gan 52900, Israel

Using bilayer films of β-Ta (5 nm)/Ni$_{0.8}$Fe$_{0.2}$ (2 nm), we fabricate elliptical structures which exhibit uniaxial magnetic anisotropy, resulting in single magnetic domain behavior. We study induced spin-orbit torques (SOTs) in these devices with first- and second-order harmonic Hall measurements for current flowing along the long axis of the ellipses and external magnetic field applied in the film plane. We observe a giant response to the SOTs associated with magnetization reversal of the NiFe layer, and we correlate it quantitatively with a $d\varphi_m/d\varphi_H$ term, where φ_m and φ_H are the in-plane angles of the magnetization and the magnetic field, respectively. We discuss theoretical and applicative implications of this intriguing behavior.

I. INTRODUCTION

Spin-orbit torques (SOTs), associated with charge-to-spin conversion, play an increasingly important role in the field of spintronics. One of the systems known to give rise to SOTs includes heavy-metal/ferromagnetic (HM/FM) heterostructures [1–9] where a charge current flowing in the HM layer induces the injection of a spin current into the FM layer owing to the spin Hall effect (SHE) within the HM and Rashba effect at the HM/FM interface. The spin currents generate two types of SOTs known as fieldlike (FL) torque $\overrightarrow{\tau}_{FL} \sim \hat{m} \times \hat{\sigma}$ and antidamping (AD) torque $\overrightarrow{\tau}_{AD} \sim \hat{m} \times (\hat{m} \times \hat{\sigma})$, where $\hat{m}$ and $\hat{\sigma}$ are the magnetic and spin-polarization unit vectors, respectively. Various effects have been used to measure SOTs such as the nonlocal spin valve which uses the SHE/inverse SHE [10,11], spin pumping by the voltage drop of the FM resonance effect [12], and the hysteresis loop shift which is based upon DC anomalous Hall effect (AHE) measurements and induced domain wall motion and nucleation at the micrometer scale [13,14].

Here, we use harmonic Hall measurements [15] which are frequently employed to determine current-induced SOTs in HM/FM heterostructures with out-of-plane [16,17] or in-plane magnetic anisotropies [18–20]. Authors of previous studies focused on measurements where the magnetization and the external magnetic field (H_{ext}) rotate coherently, i.e., when the magnitude of H_{ext} is much higher than the magnetic anisotropy (H_A) [21–24]. Here, we present angular-dependent harmonic Hall measurements for H_{ext} above and below H_A, thus exploring the limit when the magnetization rotates incoherently with H_{ext}. For fitting the results, we derive a modified form of the harmonic Hall terms applicable both in high- and low-field limits. The intriguing phenomenon reported here is a giant enhancement of the magnetic susceptibility, due to the SOTs, which occurs in the low-field limit, where the magnetization and H_{ext} do not rotate coherently. Using a modified form of the harmonic Hall terms, we fit the giant magnetic response and characterize the notable different qualitative behavior that appears in the low-field limit. The results not only give important experimental support to the more general form of the harmonic Hall equation, but they also point to a way of enhancing the magnetic response due to SOTs for future spintronic-based applications.

II. EXPERIMENTAL DETAILS

β-Ta (5 nm)/Ni$_{0.8}$Fe$_{0.2}$ (2 nm)/Ti (3 nm) heterostructures are deposited by ion-beam sputtering on a thermally oxidized Si wafer [25]. The β phase of the tantalum layer is supported by the resistivity and spin Hall angle values of $\mu\Omega$cm and $\sim$0.096, respectively [26]. Patterning is performed by several fabrication steps. A photolithography step followed by Ar-ion etching creates the pattern of the voltage and current connection lines to a cross-shaped bilayer structure. The patterning of the elliptical structure is done by two additional steps of e-beam lithography followed by Ar-ion etching. Finally, we use Au sputtering for direct attachment of the current-voltage pads to the ellipse. Here, we present measurements performed on devices where the principal axes of the ellipses are $16 \times 2\,\mu$m and $24 \times 3\,\mu$m. The experimental system consists of a rotating stage with a resolution of $0.03°$ which is placed between a pair of Helmholtz coils. A Keithley 6221/2420 and a Keithley 2182A instruments are used as the current source and nano-voltmeter, respectively. All measurements are performed at room temperature.

III. THE HARMONIC EQUATION MODEL

Commonly, the Hall voltage, measured transversely to the applied current [see Fig. 1(a)], is described as a combination of two effects, the AHE and the planar Hall effect (PHE), as follows [17]:

$$V_H = R_{AHE}I \cos(\theta_m) + \widetilde{R}_{PHE}I \sin^2(\theta_m) \sin(2\phi_m), \quad (1)$$
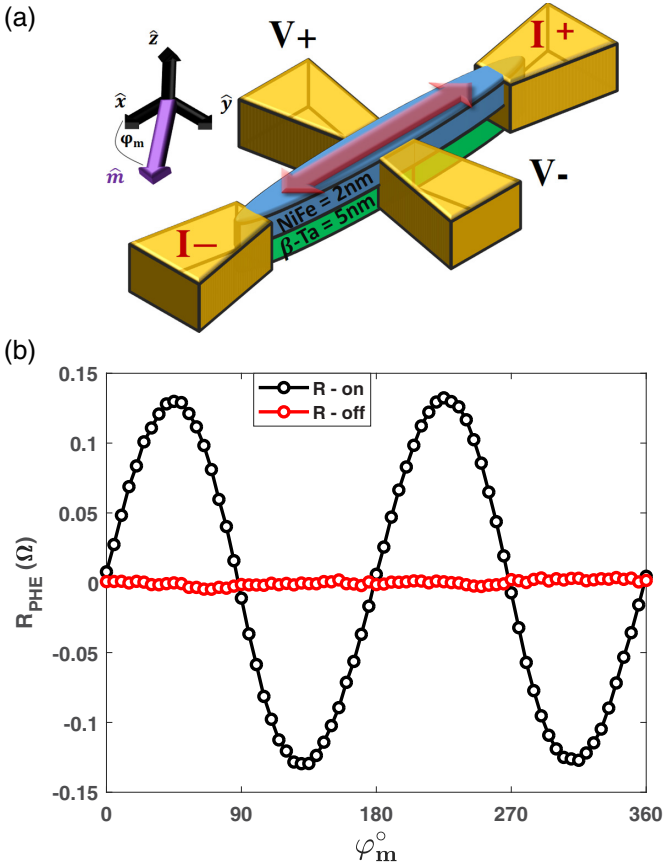
(a)

(b)

FIG. 1. A schematic of the magnetic device and basic magnetic characterization. (a) The ellipse heterostructure with the long axis connected to the bias current line and the transverse voltage measured across the short axis of the ellipse. The green layer illustrates the bottom β-Ta (5 nm), the blue layer is the $Ni_{0.8}Fe_{0.2}$ (2 nm) ferromagnetic (FM) layer, and the top Ti capping layer is not shown. (b) The planar Hall effect (PHE) on-off measurements as detailed in the text.

where R_{AHE} is the amplitude of the AHE, and $\widetilde{R}_{PHE}$ is the amplitude of the PHE. The angles φ_m and θ_m are the azimuthal and polar angles of the magnetization relative to the current direction, respectively. The current which drives the magnetic oscillation is denoted as I.

By expanding the Hall voltage in series around the equilibrium magnetization direction and separating the remaining terms according to the power of I, we obtain two harmonic terms. The first-order harmonic Hall resistance is given by

$$R_{xy} = R_{AHE}\cos(\theta_m) + \widetilde{R}_{PHE}\sin^2(\theta_m)\sin(2\phi_m). \quad (2)$$

Assuming that the Hall measurements are performed with H_{ext} sufficiently large enough to induce magnetization alignment and that the out-of plane magnetic hard axis is strong enough to keep the magnetic dynamics within the film plane, the second-order harmonic Hall signal denoted as ΔR_{xy} is given by [18]

$$\Delta R_{xy} = 2\widetilde{R}_{PHE}\cos(2\phi_m)\cos(\phi_m)\frac{H_{FL}}{H_{ext}}, \quad (3)$$

where H_{FL} is the effective field associated with a $\vec{\tau}_{FL} \sim \hat{m} \times \hat{\sigma}$ torque.

As we discuss in detail in the Supplemental Material [27] (and Ref. [28] therein), when coherent rotation cannot be assumed, the in-plane angle φ_H of H_{ext} appears explicitly in a modified form of the equation given by

$$\Delta R_{xy} = 2\widetilde{R}_{PHE}\frac{d\phi_m}{d\phi_H}\cos(2\phi_m)\cos(\phi_m)\frac{H_{FL}}{H_{ext}\cos(\phi_H - \phi_m)}. \quad (4)$$

We note that a previous derivation of Eq. (4) assumes $\phi_m \approx \phi_H$ and that the magnetization is in the film plane [18]. In our derivation, we only assume the latter, showing that it can be applicable even when there are large misalignments between the two angles.

To use Eq. (4), we determine ϕ_m as a function of ϕ_H based on the first-order harmonic R_{xy} measurements. In addition, ϕ_m is determined by using the Stoner-Wolfarth (SW) model for a single magnetic domain with uniaxial anisotropy [29]. As we show below, the two methods give consistent results, indicating that our devices behave effectively as a single magnetic domain with uniaxial magnetic anisotropy. When SW model does not apply, ϕ_m can still be determined by R_{xy}; thus, the procedure presented here of obtaining ϕ_m from R_{xy} and using it to determine ΔR_{xy} is applicable in the general case of uniform in-plane magnetization. In the following, we use both Eqs. (3) and (4) according to their relevance.

IV. RESULTS

Figure 1(a) presents a schematic illustration of our devices with the relative coordinate system used below. Figure 1(b) presents PHE resistance (R_{PHE}) measurements used for magnetic characterization [30]. Here, R_{PHE} is defined as the transverse voltage divided by the current commonly described in magnetic films by $R_{PHE} = \widetilde{R}_{PHE}\sin(2\phi_m)$ [31]. The figure shows R_{PHE} as a function of ϕ_m obtained with a saturating field of 100 Oe and after the field is turned off at each field angle. The device exhibits shape-induced uniaxial magnetic anisotropy (H_A) along the long axis of the ellipse, as evident from the zero-field plateau. A value of $H_A \cong 10$ Oe is determined from the slope of R_{PHE} vs the perpendicular component of the external magnetic field [32] (see Fig. S1 in the Supplemental Material [27] for details).

When the applied magnetic field is less than a saturating field, we can still determine ϕ_m by using the relation of $\phi_m = \frac{1}{2}\sin^{-1}(R_{PHE}/\widetilde{R}_{PHE})$. Figures 2(a) and 2(b) display the first-order harmonic term R_{xy}, which is equal to R_{PHE} in in-plane magnetized structures [insert $\theta_m = 90°$ into Eq. (2)], and ϕ_m as a function of the angle ϕ_H at which the external in-plane magnetic field is applied. The solid lines are fits of R_{xy} and ϕ_m as a function of ϕ_H using the SW model. The quality of the fits indicates that our elliptical devices behave effectively as single magnetic domains with uniaxial magnetic anisotropy. A bias current of 2 mA ($J_{\beta\text{-Ta}} = 0.75 \times 10^7$ A/cm^2) is applied in all measurements of Figs. 2 and 3.

Figure 2(a) shows that, for $H_{ext} \gg H_A$, the magnetization and the external magnetic field rotate coherently, yielding $R_{xy} = R_{PHE} \propto \sin(2\phi_m)$ [Eq. (2) for $\theta_m = 90°$]. As H_{ext} decreases and the magnetic anisotropy H_A becomes more
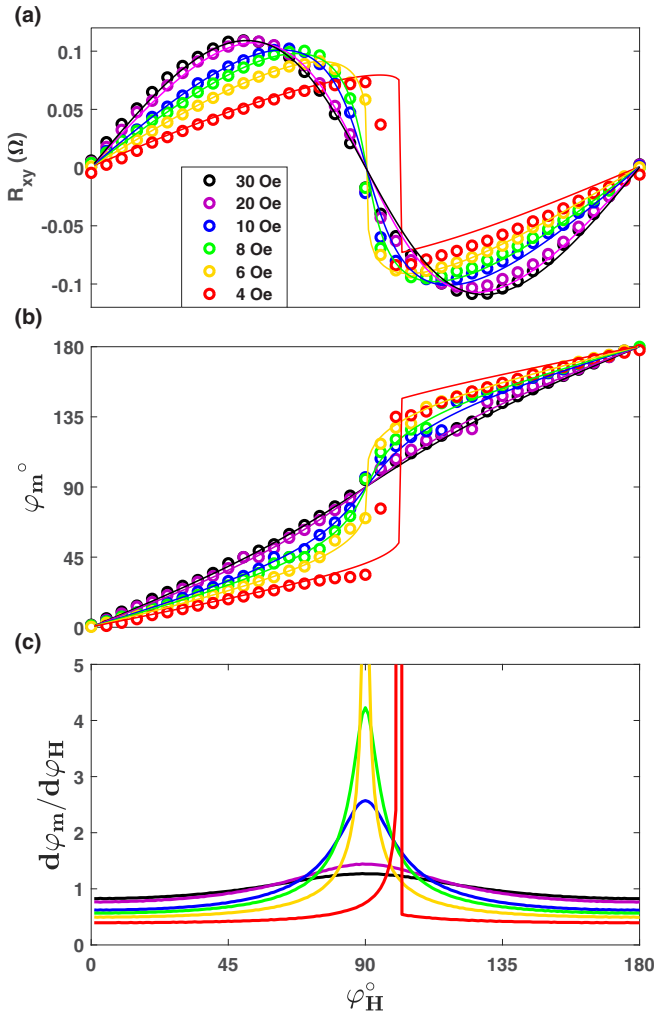
FIG. 2. (a) R_{xy}, (b) ϕ_m, and (c) $d\phi_m/d\phi_H$ as a function of the angle ϕ_H at which H_{ext} is applied. The continuous lines are Stoner-Wolhfarth (SW) fits to the experimental data points.

dominant, the magnetization rotation stops being continuous, and discontinuous jumps are observed. The discontinuous rotating magnetization skips intermediate magnetic orientations between the easy and hard axes, yielding a reduced peak value for R_{xy}. Consequently, the overall amplitude of R_{xy} decreases. We note that the discontinuous magnetization is characterized by regimes of *suppressed* ($d\phi_m/d\phi_H < 1$) and *accelerated* ($d\phi_m/d\phi_H > 1$) rotations.

Figure 2(b) shows the deviation from coherent rotation with H_{ext} by presenting ϕ_m vs ϕ_H. When $H_{ext} \gg H_A$, we approach coherent rotation. As the field decreases, two separate quasilinear regions appear associated with the tendency of the magnetization to align with the easy axis on both sides of the hard axis. The location of the two regions varies with H_{ext}. As H_{ext} decreases, the magnetization jump occurs at higher values of ϕ_H, i.e., the transition between the two quasilinear regions is shifted to a higher field angle. Furthermore, the range of change of ϕ_m in the two quasilinear regions shrinks. For instance, when $H_{ext} = 4$ Oe, the magnetization orientation does not exceed $33°$ before jumping to the other side of the hard axis.

Figure 2(c) displays $d\phi_m/d\phi_H$, which as we show below can become essential for understanding the second-order harmonic Hall term ΔR_{xy} [Eq. (4)]. For $H_{ext} \gg H_A$, $d\phi_m/d\phi_H = 1$, and Eq. (3) applies. As H_{ext} decreases and approaches H_A, a suppressed rotation region where $d\phi_m/d\phi_H < 1$ and an accelerated region where $d\phi_m/d\phi_H > 1$ appear. We focus on the accelerated regions where $d\phi_m/d\phi_H$ increases significantly. This value of $d\phi_m/d\phi_H$ determines the magnetic response to an in-plane SOT-induced field, as seen in Eq. (4). The fits in Fig. 2(c) which are based on the SW model (with $\Delta\phi_H = 3°$) yield a maximum value of $d\phi_m/d\phi_H = 2.5$ for $H_{ext} = H_A$ and $d\phi_m/d\phi_H \sim 30$ for $H_{ext} = 0.4 H_A = 4$ Oe.

The term $d\phi_m/d\phi_H$ is analytically defined only when the derivative exists, which is not the case when first-order magnetization processes [33] such as discontinuous jumps in ϕ_m exist. Using the SW model, we find that, below $H_{ext} \cong 0.7$ H_A (~ 7 Oe in our case), a discontinuous jump in the magnetization orientation is expected to appear consistent with previous reports [34,35]. Figure 2(c) shows a giant increase of $d\phi_m/d\phi_H$ when ϕ_H exceeds the hard axis direction for fields below the critical field value of 7 Oe, namely, for fields of 4 and 6 Oe. Theoretically, for this field range, we expect a singularity in the magnetization curve, i.e., $d\phi_m/d\phi_H$ diverging to infinity [36]. However, imperfections suppress the expected divergence. The existence of the singularity is independent of the type of hard direction (hard axis or hard plane); therefore, the procedure presented here and our conclusions are relevant to any type of magnetic anisotropy (magnetocrystalline anisotropy [37], FM/antiferromagnetic interfacial anisotropy [38]) if the magnetization remains uniform.

We turn now to our main results and present the qualitative and quantitative changes in the second-order harmonic Hall measurements going from the limit of coherent magnetization rotation where $\phi_m = \phi_H$ to the lower field limit where the suppressed ($d\phi_m/d\phi_H < 1$) and accelerated ($d\phi_m/d\phi_H > 1$) regions of the magnetization rotation appear. Figures 3(a)–3(f) show the second-order harmonic Hall term ΔR_{xy} as a function of the in-plane angle ϕ_H at which an external magnetic field is applied. For DC measurements, ΔR_{xy} is given by [39–44]

$$\Delta R_{xy} = \frac{V_{Hall}(+I) + V_{Hall}(-I)}{2I}, \tag{5}$$

and we use Eq. (4) to fit the data. The angle ϕ_m used in the fit can be extracted either from R_{xy} or the SW model whose applicability is demonstrated in Fig. 2. Figures 3(a) and 3(b) show ΔR_{xy} for $H_{ext} \gg H_A$, and thus, their shape matches previous reports [19]. As H_{ext} decreases, ΔR_{xy} varies qualitatively and quantitatively. A direct quantitative effect is due to the term $1/H_{ext}$ in the prefactor of ΔR_{xy}. The indirect effect is manifested in the quantitative and qualitative behavior of

$$\frac{d\phi_m}{d\phi_H} \frac{\cos(2\phi_m)\cos(\phi_m)}{\cos(\phi_H - \phi_m)}. \tag{6}$$

The $\cos(\phi_m - \phi_H)$ term does not appear in Eq. (3) since, in the high field limit, it is equal to 1, like $d\phi_m/d\phi_H$. When Eq. (4) is applicable, we find that the largest gap between ϕ_m and ϕ_H is immediately before and after the singularity. See Fig. S2 in the Supplemental Material [27] for the related discussion regarding the gap between the two angles and its
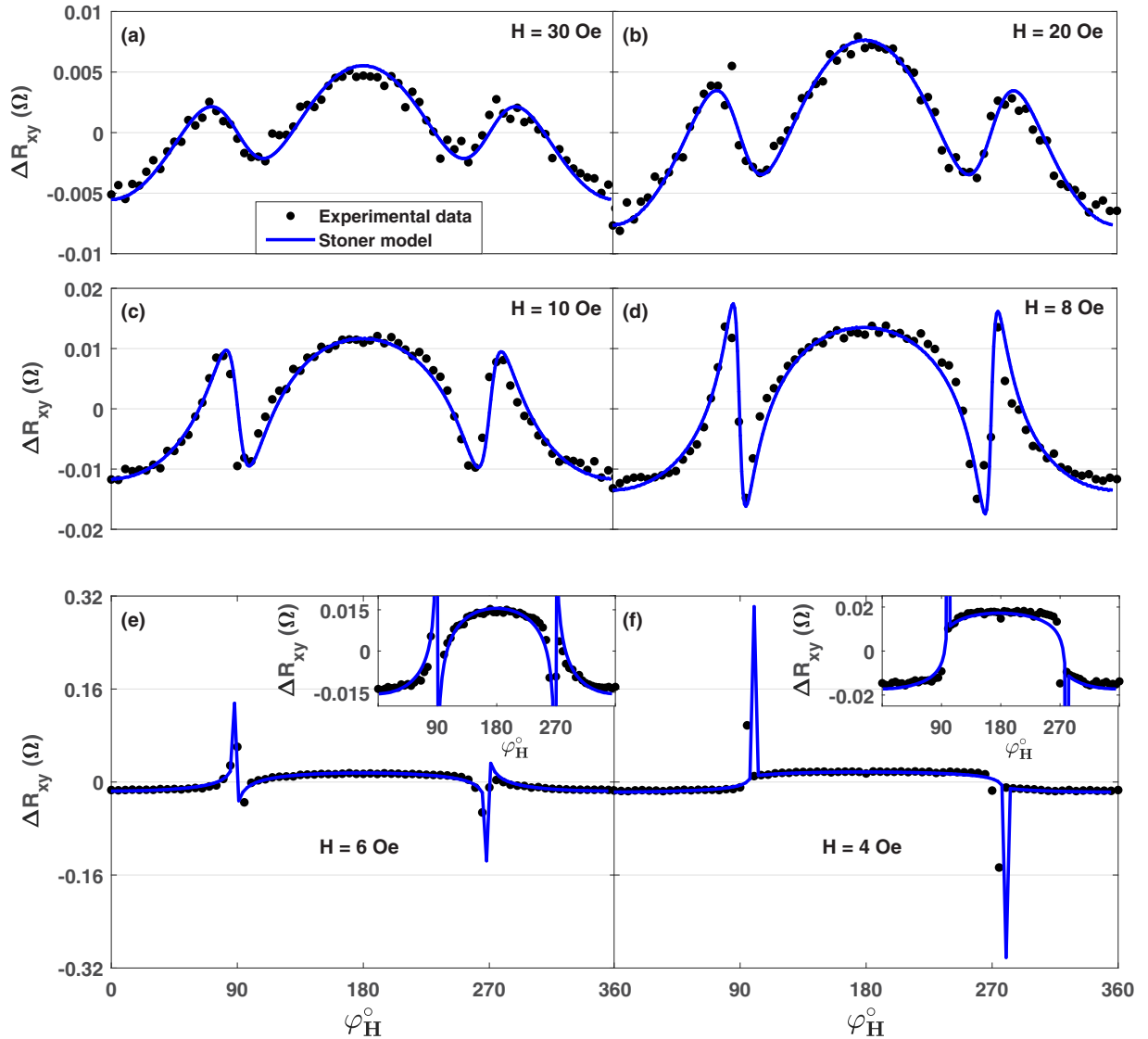
FIG. 3. ΔR_{xy} vs ϕ_H for H_{ext} ranging between 4 and 30 Oe. The black circles are experimental data points. The blue lines are fits where ϕ_m and the expected corresponding ΔR_{xy} are extracted by using the Stoner-Wolhfarth (SW) model.

limited implications on ΔR_{xy}. As we show now, the dominant term which is responsible for the dramatic qualitative and quantitative changes is $d\phi_m/d\phi_H$.

The effect of $d\phi_m/d\phi_H$ on ΔR_{xy} varies considerably during the magnetization rotation. In the suppressed rotation regime, $d\phi_H/d\phi_m$ reduces ΔR_{xy}. In this rotation regime, as H_{ext} decreases, $d\phi_H/d\phi_m$ converges into a constant value [Fig. 2(c)]. Therefore, in the suppressed rotation regime, ΔR_{xy} is given by the term of Eq. (3) multiplied by a constant <1 and the term of $\cos^{-1}(\phi_m - \phi_H)$ which remains ~ 1 (see Fig. S2 in the Supplemental Material [27] for details). Consequently, in this regime, the behavior of ΔR_{xy} is qualitatively like its behavior in the high-field limit, which is representable solely with Eq. (3). In the accelerated rotation regime, the contribution of $d\phi_m/d\phi_H$ to ΔR_{xy} is dramatic and dominant. Overall, Figs. 3(c) and 3(d) represent measurements when $d\phi_H/d\phi_m$ becomes the dominant contribution of ΔR_{xy}, but still the signal of ΔR_{xy} in the accelerated regimes is on the same order as the signal of ΔR_{xy} in the suppressed regimes.

Further decrease of H_{ext} yields the behavior presented in Figs. 3(e) and 3(f), where the value of $d\phi_H/d\phi_m$ in the accelerated regime increases drastically. Due to the relation of $d\phi_H/d\phi_m$ and H_{FL} with ΔR_{xy}, these results manifest a giant magnetic response to SOTs associated with abrupt magnetization rotation across the hard axis. We note that the Oersted fields due to currents in the β-Ta and Ti layers can yield a similar response. However, in our case, the estimated contribution is expected to yield a response with an opposite sign. We also note that the fields used in the measurement presented in Figs. 3(e) and 3(f) are smaller than the theoretically expected minimal field required for magnetization singularity, and we do not observe such a singularity since our devices are not ideal uniaxial domains. The insets of Figs. 3(e) and 3(f) show the results with a smaller y-axis range to demonstrate that, outside of the accelerated regimes, ΔR_{xy} is qualitatively and quantitatively like the behavior of ΔR_{xy} in the high-field limit. Interestingly, as shown in Fig. S4 in the Supplemental Material [27], when smaller H_{ext} are used, the system becomes

a two-level system with two plateaus separated by the giant magnetic response.

V. SUMMARY

We perform harmonic Hall measurements to study the SOTs in HM/FM devices with shape-induced uniaxial magnetic anisotropy. We find that the magnetic response to the SOT becomes giant as H_{ext} approaches H_A and the magnetiza-tion reversal becomes sharper. We attribute this behavior to the derived dependence of the second-order harmonic Hall signal on $d\phi_m/d\phi_H$ and show good agreement with the modified set of harmonic Hall equations we present. Whereas theoretically $d\phi_m/d\phi_H$ is expected to diverge as the magnetization rotation approaches a discontinuous jump, experimentally, $d\phi_m/d\phi_H$ is bounded due to imperfections. We believe that our results pave a route for a significant enhancement of the magnetic susceptibility when SOT is present which may be useful for developing spintronic devices.

[1] M. Dyakonov and V. Perel, Phys. Lett. A **35**, 459 (1971).

[2] J. E. Hirsch, Phys. Rev. Lett. **83**, 1834 (1999).

[3] S. Zhang, Phys. Rev. Lett. **85**, 393 (2000).

[4] J. Sinova, D. Culcer, Q. Niu, N. A. Sinitsyn, T. Jungwirth, and A. H. MacDonald, Phys. Rev. Lett. **92**, 126603 (2004).

[5] Y. K. Kato, R. C. Myers, A. C. Gossard, and D. D. Awschalom, Science **306**, 1910 (2004).

[6] V. Sih, W. H. Lau, R. C. Myers, V. R. Horowitz, A. C. Gossard, and D. D. Awschalom, Phys. Rev. Lett. **97**, 096605 (2006).

[7] S. O. Valenzuela and M. Tinkham, Nature (London) **442**, 176 (2006).

[8] T. Kimura, Y. Otani, T. Sato, S. Takahashi, and S. Maekawa, Phys. Rev. Lett. **98**, 156601 (2007).

[9] A. Manchon, J. Železný, I. M. Miron, T. Jungwirth, J. Sinova, A. Thiaville, K. Garello, and P. Gambardella, Rev. Mod. Phys. **91**, 035004 (2019).

[10] Y. Niimi and Y. Otani, Rep. Prog. Phys. **78**, 124501 (2015).

[11] T. Kimura, J. Hamrle, and Y. Otani, Phys. Rev. B **72**, 014461 (2005).

[12] M. V. Costache, S. M. Watts, M. Sladkov, C. H. van der Wal, and B. J. van Wees, Appl. Phys. Lett. **89**, 232115 (2006).

[13] C.-F. Pai, M. Mann, A. J. Tan, and G. S. D. Beach, Phys. Rev. B **93**, 144409 (2016).

[14] S. Emori, E. Martinez, K.-J. Lee, H.-W. Lee, U. Bauer, S.-M. Ahn, P. Agrawal, D. C. Bono, and G. S. D. Beach, Phys. Rev. B **90**, 184427 (2014).

[15] U. H. Pi, K. Won Kim, J. Y. Bae, S. C. Lee, Y. J. Cho, K. S. Kim, and S. Seo, Appl. Phys. Lett. **97**, 162507 (2010).

[16] J. Kim, J. Sinha, M. Hayashi, M. Yamanouchi, S. Fukami, T. Suzuki, S. Mitani, and H. Ohno, Nat. Mater. **12**, 240 (2013).

[17] K. Garello, I. M. Miron, C. O. Avci, F. Freimuth, Y. Mokrousov, S. Blügel, S. Auffret, O. Boulle, G. Gaudin, and P. Gambardella, Nat. Nanotechnol. **8**, 587 (2013).

[18] C. O. Avci, K. Garello, M. Gabureac, A. Ghosh, A. Fuhrer, S. F. Alvarado, and P. Gambardella, Phys. Rev. B **90**, 224427 (2014).

[19] Y. Wen, J. Wu, P. Li, Q. Zhang, Y. Zhao, A. Manchon, J. Q. Xiao, and X. Zhang, Phys. Rev. B **95**, 104403 (2017).

[20] N. Roschewsky, E. S. Walker, P. Gowtham, S. Muschinske, F. Hellman, S. R. Bank, and S. Salahuddin, Phys. Rev. B **99**, 195103 (2019).

[21] M. Hayashi, J. Kim, M. Yamanouchi, and H. Ohno, Phys. Rev. B **89**, 144425 (2014).

[22] Y. Du, R. Thompson, M. Kohda, and J. Nitta, AIP Adv. **11**, 025033 (2021).

[23] S. Novakov, B. Jariwala, N. M. Vu, A. Kozhakhmetov, J. A. Robinson, and J. T. Heron, ACS Appl. Mater. Interfaces **13**, 13744 (2021).

[24] M. Alghamdi, M. Lohmann, J. Li, P. R. Jothi, Q. Shao, M. Aldosary, T. Su, B. P. T. Fokwa, and J. Shi, Nano Lett. **19**, 4400 (2019).

[25] S. Cardoso, V. Gehanno, R. Ferreira, and P. Freitas, IEEE Trans. Magn. **35**, 2952 (1999).

[26] S. Das, L. Avraham, Y. Telepinsky, V. Mor, M. Schultz, and L. Klein, Sci. Rep. **8**, 15160 (2018).

[27] See Supplemental Material at https://link.aps.org/supplemental/10.1103/PhysRevB.106.214401 for details about the derivation of the main equations and additional information.

[28] S. Karimeddiny, J. A. Mittelstaedt, R. A. Buhrman, and D. C. Ralph, Phys. Rev. Appl. **14**, 024024 (2020).

[29] C. Tannous and J. Gieraltowski, Eur. J. Phys. **29**, 475 (2008).

[30] Y. Telepinsky, V. Mor, M. Schultz, and L. Klein, J. Appl. Phys. **111**, 07C715 (2012).

[31] V. D. Ky, Phys. Stat. Sol. (b) **26**, 565 (1968).

[32] V. Mor, J. Appl. Phys. **111**, 07E519 (2012).

[33] L. Pareti, F. Bolzoni, and O. Moze, Phys. Rev. B **32**, 7604 (1985).

[34] V. Kalita, M. Kulyk, and S. Ryabchenko, Low Temp. Phys. **43**, 359 (2017).

[35] A. Chen, K. Guslienko, and J. Gonzalez, J. Appl. Phys. **108**, 083920 (2010).

[36] G. Asti and F. Bolzoni, J. Appl. Phys. **58**, 1924 (1985).

[37] J. Geshev, L. G. Pereira, and J. E. Schmidt, Phys. Rev. B **66**, 134432 (2002).

[38] G. Asti, F. Bolzoni, and R. Cabassi, J. Appl. Phys. **73**, 323 (1993).

[39] Z. Luo, Q. Zhang, Y. Xu, Y. Yang, X. Zhang, and Y. Wu, Phys. Rev. Appl. **11**, 064021 (2019).

[40] R. Guerrero, A. Anadón, A. Gudín, J. M. Diez, P. Olleros-Rodríguez, M. Muñoz, R. Miranda, J. Camarero, and P. Perna, arXiv:2004.02695.

[41] Y. Xu, Y. Yang, K. Yao, B. Xu, and Y. Wu, Sci. Rep. **6**, 26180 (2016).

[42] X. Fan, J. Wu, Y. Chen, M. J. Jerry, H. Zhang, and J. Q. Xiao, Nat. Commun. **4**, 1799 (2013).

[43] X. Fan, H. Celik, J. Wu, C. Ni, K.-J. Lee, V. O. Lorenz, and J. Q. Xiao, Nat. Commun. **5**, 3042 (2014).

[44] S. Emori, T. Nan, A. M. Belkessam, X. Wang, A. D. Matyushov, C. J. Babroski, Y. Gao, H. Lin, and N. X. Sun, Phys. Rev. B **93**, 180402(R) (2016).